OPEN ACCESS Freely available online

PLOS ONE

Growth, Structure, Thermal Properties and Spectroscopic Characteristics of Nd^{3+}-Doped $KGdP_4O_{12}$ Crystal

Tongqing Sun[1,2]*, Yu Zhang[2], Pai Shan[2], Zichang Zhang[2], Shaolin Chen[1,3], Yongfa Kong[1,2,3], Jingjun Xu[1,2,3]

1 The MOE Key Laboratory of Weak-Light Nonlinear Photonics, Nankai University, Tianjin, People's Republic of China, **2** School of Physics, Nankai University, Tianjin, People's Republic of China, **3** TEDA Applied Physics Institute, Nankai University, Tianjin, People's Republic of China

Abstract

A single crystal of Nd^{3+}-doped $KGdP_4O_{12}$ was successfully grown with the top-seeded solution growth and slow cooling (TSSG−SC) technique. It crystallizes in space group $C2/c$ with cell parameters $a = 7.812(2)$ Å, $b = 12.307(3)$ Å, $c = 10.474(2)$ Å, $\beta = 110.84(3)^\circ$ and $Z = 4$. The IR and Raman spectra also indicated that the phosphoric polyhedra of Nd:$KGdP_4O_{12}$ has a cyclic symmetry. The chemical composition of the crystal was analyzed and the distribution coefficient of Nd^{3+} was calculated. The crystal morphology of $KGdP_4O_{12}$ was identified using X-ray diffraction. The compound has good thermal stability to 920°C. Its specific heat and thermal conductivity were determined for potential applications. The spectral properties of Nd:$KGdP_4O_{12}$ indicates that it exhibits broad absorption and emission bands, which are attributed to low symmetry of the crystal. The broad absorption band around 798 nm has a full-width at half-maximum (FWHM) of 14.8 nm and is suitable for AlGaAs laser diode pumping. Moreover, 5 at% Nd^{3+}-doped $KGdP_4O_{12}$ crystal has a long luminescence lifetime of 300 μs and a high quantum efficiency of 96%.

Citation: Sun T, Zhang Y, Shan P, Zhang Z, Chen S, et al. (2014) Growth, Structure, Thermal Properties and Spectroscopic Characteristics of Nd^{3+}-Doped $KGdP_4O_{12}$ Crystal. PLoS ONE 9(6): e100922. doi:10.1371/journal.pone.0100922

Editor: Andreas Hofmann, Griffith University, Australia

Received January 21, 2014; **Accepted** June 2, 2014; **Published** June 26, 2014

Funding: This work is supported by the National Natural Science Foundation of China (Grant No. 21271109) and the Fundamental Research Funds for the Central Universities of China (65122011). The funders had no role in study design, data collection and analysis, decision to publish, or preparation of the manuscript.

Competing Interests: The authors have declared that no competing interests exist.

* Email: suntq@nankai.edu.cn

Introduction

With the development of the diode-pumped solid-state (DPSS) lasers based on neodymium-doped crystals, research on new laser host materials has gained much interest [1]. Nd:YAG crystal is still the most common Nd^{3+} laser material because of its good physical and laser properties, but it is limited to low Nd^{3+}-doped concentration and narrow absorption bandwidth near the AlGaAs diode emission wavelength of 808 nm. Because the emission wavelength of the laser diode increases at 0.2−0.3 $nm \cdot K^{-1}$ of the laser device, the temperature stability of the laser diode needs to be tightly controlled. Therefore, it is necessary to explore new and more efficient crystals for DPSS lasers. Furthermore, the absorption band of laser crystals close to the laser output of AlGaAs ($\lambda = 808$ nm) needs to have a large full-width at half-maximum (FWHM).

Recently, some Nd^{3+}-doped laser crystals with broad absorption bands have been reported. They include host crystals with disordered structures such as $NaLn(WO_4)_2$ (Ln = Y or Gd, $I4_1/a$) [2,3], $SrLaGa_3O_7$ ($P\bar{4}2_1m$) [4], $Ca_3La_2(BO_3)_4$ ($Pnma$) [5], $Li_3Ba_2Ln_3(MO_4)_8$ (Ln = Y, La or Gd, M = W or Mo, $C2/c$) [6−11], $KBaGd(MO_4)_3$ (M = W or Mo, $C2/c$) [12,13] and $CaNb_2O_6$ ($Pbcn$) [14]. These species can induce inhomogeneous broadening of optical spectra from a disordered crystal lattice. Mixed crystals such as garnet $(Lu_xY_{1-x})_3Al_5O_{12}$ [15] and rare earth oxyorthosilicate Ln_2SiO_5 ($C2/c$) ($LuYSiO_5$, $GdYSiO_5$ and $LuGdSiO_5$) [16−18] can enhance the structure disorder. Many of the host crystals above have low symmetry, especially the monoclinic system $C2/c$ space group. Due to the strong anisotropy of their physical properties and biaxiality, host crystals with low symmetry may enrich spectroscopic properties of doped active ions [19].

The title compound, $KGdP_4O_{12}$, belongs to the broader family of condensed phosphates including those double phosphates of alkali and lanthanide ions with the general formula $M^{I}Ln^{III}(PO_3)_4$. The structure of $M^{I}Ln^{III}(PO_3)_4$ is highly dependent not only on the sizes of the alkali and the lanthanide ions but also on the crystallization environment. Double tetra-metaphosphates of potassium and gadolinium have low symmetry (monoclinic system) including three structural types with different space groups: $P2_1$, $P2_1/n$ and $C2/c$. The first two types are written as $KGd(PO_3)_4$ in general and are double polyphosphates. Here, the phosphoric anions have a long-chain geometry of $(PO_3)_n^{n-}$. The $C2/c$ is a cyclotetraphosphate, and these phosphoric anions have a cyclic geometry of $[P_4O_{12}]^{4-}$; hence its formula is usually written as $KGdP_4O_{12}$. The growth and structure of $KGd(PO_3)_4$ ($P2_1$) crystal was reported by Parreu et al [20,21] and it is isostructural to $KNd(PO_3)_4$ [22]–a famous Nd stoichiometric laser material. The $KGd(PO_3)_4$ ($P2_1$) can be used as a self-frequency doubling (SFD) laser host material because of its noncentrosymmetrical structure and has attracted more attention [23−26]. $KGdP_4O_{12}$ crystallized in space group $C2/c$ and $KGd(PO_3)_4$ in $P2_1/n$ were successively synthesized in phosphoric acid by Naïli et al [27,28].

Compared to other double phosphates of alkali and lanthanide ions with the general formula $M^{I}Ln^{III}(PO_3)_4$, $KGdP_4O_{12}$ has the following characteristics as a new laser host material. First, Gd^{3+} is much closer to Nd^{3+} in size; hence $KGdP_4O_{12}$ is easily substituted

with Nd^{3+}. Second, raw materials for preparing $KGdP_4O_{12}$ are easily available and very cheap in comparison with double metaphosphates of cesium or rubidium. Third, the spectroscopic spectrum of doped active ions may be broadened because of its low symmetry in the space group $C2/c$. Finally, the $KGdP_4O_{12}$ crystal has a cyclic geometry that is difficult to cleave in contrast with compounds having long chain geometry.

To the best of our knowledge, the crystal growth of $KGdP_4O_{12}$ has not yet been reported. Here, we have grown a single crystal of Nd^{3+}-doped $KGdP_4O_{12}$ with high quality and determined its structural character to be a cyclic geometry via single crystal structural analysis and IR and Raman spectroscopy. The spectral characteristics of the Nd:$KGdP_4O_{12}$ crystal were studied through its absorption spectrum, emission and excitation fluorescent spectra, and fluorescence decay curve. Finally, we measured its thermal stability, specific heat and thermal conductivity.

Materials and Methods

1. Crystal growth

The crystal growth used a single-zone vertical tubular electric furnace with a Kantal AF heater. The temperature of the furnace was measured near the heater with a B-type thermocouple and was regulated with a SHIMADEN FP21 type temperature controller.

We grew Nd:$KGdP_4O_{12}$ crystals with the top-seeded solution growth and slow cooling (TSSG−SC) technique from a self-flux. The starting material was prepared by mixing Nd_2O_3 (4N), Gd_2O_3 (4N), K_2CO_3 (99.0%) and $NH_4H_2PO_4$ (99.0%) at a molar ratio of 0.05:0.95:3:12 in an agate mortar. This was then transferred into a

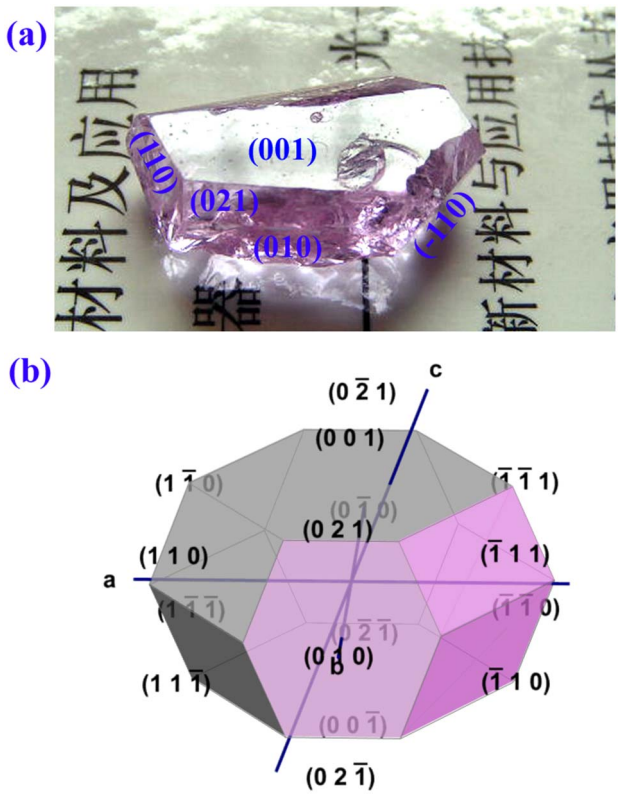

Figure 1. Photograph (a) of the as-grown single crystal with a size of 20 mm×10 mm×5 mm and the theoretical morphology (b) of the Nd:$KGdP_4O_{12}$ crystal.
doi:10.1371/journal.pone.0100922.g001

$\Phi 60\times 60$ mm^2 Pt crucible to melt in batches. During the melting, a stoichiometric Nd_2O_3, Gd_2O_3, K_2CO_3 and $NH_4H_2PO_4$ generated the title compound $KGd_{0.95}Nd_{0.05}P_4O_{12}$. An excess of K_2CO_3 and $NH_4H_2PO_4$ reacted to produce potassium metaphosphate compound, which served as a self-flux to avoid foreign ions during the crystal growth. The typical chemical reactions are shown below.

$$K_2CO_3+0.95Gd_2O_3+0.05Nd_2O_3+8NH_4H_2PO_4 \rightarrow 2KGd_{0.95}Nd_{0.05}P_4O_{12}+8NH_3\uparrow+CO_2\uparrow+12H_2O\uparrow$$

$$K_2CO_3+2NH_4H_2PO_4 \rightarrow 2KPO_3+2NH_3\uparrow+CO_2\uparrow+3H_2O\uparrow$$

There was marked bubbling of NH_3, CO_2 and H_2O, and the mixture was heated slowly to a melt. The melt was homogenized at 900°C with a stirrer until the melt was clear and there were no bubbles. Meanwhile, the crucible was rotated alternately clockwise and counterclockwise at 15 revolutions per minute for complete homogenization. The oscillating crucible rotation was also necessary during the crystal growth for effective mass transport. The coldest position in the solution was 0.5 cm below the melt surface and the temperature gradient in the axial direction was $1.3°C\cdot cm^{-1}$. After several attempts, the melt temperature decreased to 812°C. Meanwhile, a thick wire of platinum attached to a corundum rod was introduced into the furnace and was placed above the melt. About 10 min later, the platinum wire was immersed below the melt surface as a seed. While maintaining the oscillating crucible rotation, the melt temperature was reduced at $0.4°C\cdot d^{-1}$ until it reached 794°C. During this process, the solute first crystallized on the platinum wire, which served as the seed for larger crystals.

After the growth was completed, the crystals were removed from the solution. The furnace was cooled to room temperature slowly and then some single crystals clustering around the platinum wire were taken out of the furnace. Figure 1(a) shows that the biggest one of these had good transparency with no cracks or inclusions. The colour of the crystal shows that the neodymium ion had already entered the crystal lattice. The stoichiometry of the crystal was analyzed by inductively coupled plasma−atomic emission spectrometer (ICP−AES) (Thermo IRIS Advantage). The density of the Nd:$KGdP_4O_{12}$ crystal at room temperature (23°C) was measured using a density unit of Sartorius balance (YDK01−C) by the buoyancy method.

2. X-ray diffraction analysis

The X-ray diffraction (XRD) technique was used to analyze several aspects of the as-grown Nd:$KGdP_4O_{12}$ single crystal such as determining its structure, identifying the crystalline phase, studying the crystal morphology as well as crystallinity.

A single crystal of Nd:$KGdP_4O_{12}$ cut from the as-grown crystal was used for indexing and intensity data collections on a Rigaku Saturn CCD area detector diffractometer using Mo $K\alpha$ graphite monochromated radiation ($\lambda = 0.71073$ Å). The structure was resolved with the SHELXS-97 computer utility, and refined by a full-matrix least-squares method with SHELXL-97 software.

Polycrystalline powder of Nd:$KGdP_4O_{12}$ was prepared from the as-grown single crystal. The powder X-ray diffraction (PXRD) pattern of Nd:$KGdP_4O_{12}$ was recorded at room temperature with a Fangyuan DX2700 (Dandong, China) powder diffractometer using graphite monochromatized Cu $K\alpha$ radiation in the 2θ range 10°−70° with a step of 0.02°.

An XRD goniometer was used to identify and orientate the crystalline forms that comprised the morphological habit for the

Table 1. The result of chemical analysis for the as-grown crystal of 5 at% Nd^{3+}-doped $KGdP_4O_{12}$.

Element (mass%)	K (%)	Gd (%)	Nd (%)	P (%)
Calculated	7.64	29.20	1.41	24.22
Experimental	7.27	28.98	1.38	23.86

doi:10.1371/journal.pone.0100922.t001

as-grown single crystal had well-developed facets. XRD was also used to check the quality of the as-grown Nd:$KGdP_4O_{12}$ crystal. The crystal in Figure 1(a) was polished and used as a sample. The rocking curve of the (004) diffraction crystal face was obtained on an XRD diffractometer (PANalytical X'Pert PRO) equipped with a four-crystal Ge (022) monochromator. The setting of the X-ray tube (PW3373/10) was 40 kV and 10 mA. The step time and step size were 0.1 s and 0.001°, respectively.

3. IR and Raman spectroscopy

The molecular spectroscopy and lattice vibrations of Nd:$KGdP_4O_{12}$ were studied with Fourier transform infrared (FTIR) and Raman spectroscopy. The IR spectrum of a KBr pressed pellet of the powered sample was recorded from 4000 to 400 cm^{-1} on a Nicolet Magna-IR 560 ESP FTIR spectrometer. The as-grown crystal shown in Figure 1(a) was also studied on a Renishaw inVia Raman microscope. The output wavelength of the excited CW argon laser was 514 nm.

4. Thermal analysis

The thermal stability of Nd:$KGdP_4O_{12}$ was measured with both thermogravimetry and differential scanning calorimetry (TG–DSC) using a Netzsch STA 449C from 40 to 1000°C at 10°C·min^{-1}. The specific heat of the Nd:$KGdP_4O_{12}$ crystal was also measured by DSC using a simultaneous thermal analyzer (Netzsch DSC 200 F3) in an atmosphere of N_2.

The thermal diffusivity was measured by the laser flash method using a laser flash apparatus (Netzsch LFA 457 Nanoflash) in the 25–300°C range at intervals of 50°C. A 0.95 mm×4 mm×4 mm sample was used to carry out the measurements whose {001} faces were polished and coated with graphite on both sides.

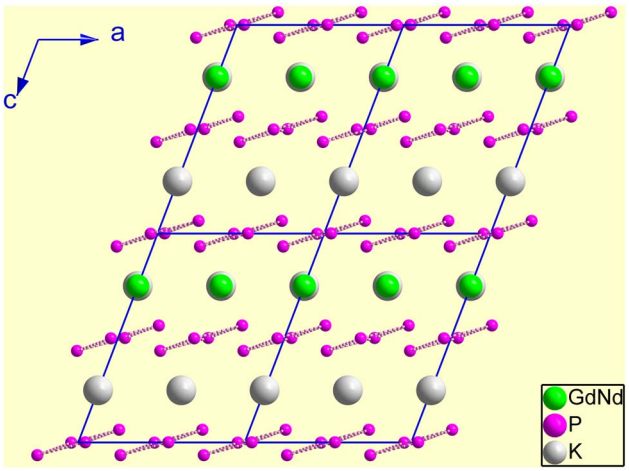

Figure 2. Structure projection of Nd:$KGdP_4O_{12}$ along the [010] direction. (Here, all the oxygen atoms have been omitted.).
doi:10.1371/journal.pone.0100922.g002

5. Spectroscopic characterization

A 4.30-mm thick sample was polished and used to measure the spectroscopic properties. The polished facet was {001}. The unpolarized absorption spectrum was measured on a Hitachi UV–Vis–NIR spectrophotometer (U4100) from 175 to 2000 nm. The fluorescence spectra were recorded using an Edinburgh Instruments FLS920 spectrophotometer with a xenon lamp as the excitation source. The incident light and fluorescence were dispersed with two M300 monochromators using ruling gratings from Bentham Instruments. A cooled Hamamatsu R5509-72 photomultiplier was used for detection. The decay curve was measured using a pulsed xenon lamp as the pump source. The pulse duration was 10 ns, and the excitation wavelength was 808 nm. All the measurements were performed at room temperature (300 K). The splitting of the Nd^{3+} emission band was also studied at 10 K using the same FLS920 spectrophotometer equipped with a close cycle helium cryostat (Advanced Research Systems DE202).

Results and Discussion

1. Crystal growth and chemical composition

As mentioned above, $KGdP_4O_{12}$ is a polymorphous compound. In addition to the $C2/c$ phase, it has two isomers, i.e. $KGd(PO_3)_4$ in $P2_1$ and $P2_1/n$. Both $KGdP_4O_{12}$ in $C2/c$ and $KGd(PO_3)_4$ in $P2_1/n$ can be prepared by crystallizing KH_2PO_4 and Gd_2O_3 from phosphoric acid below 550°C [27,28]. Because of the lower crystallization temperature and the resulting higher viscosity, it is difficult to grow bulk crystals of Nd:$KGdP_4O_{12}$. Parreu grew a $KGd(PO_3)_4$ crystal in $P2_1$ from a melt made from $NH_4H_2PO_4$, K_2CO_3 and Gd_2O_3 at a higher temperature [20]. In studying the crystallization region of $KGd(PO_3)_4$ ($P2_1$) in the ternary system Gd_2O_3–K_2O–P_2O_5, six neighbouring phases were found, and $KGdP_4O_{12}$ in $C2/c$ was one of them. By choosing the ratio in the melt composition, we successfully grew bulk crystals of Nd:$KGdP_4O_{12}$ (Figure 1(a)). The composition of a melt influences the formation of phase. A similar situation occurred to a $BaTeMo_2O_9$ polymorphous compound recently reported–the α and β crystal phases can be grown from a melt with different compositions [29].

The chemical composition of the as-grown crystal was analyzed by ICP–AES (Table 1). The chemical formula of the crystal corresponds to $KGd_{0.95}Nd_{0.05}P_4O_{12}$, which is consistent with results of single crystal diffraction. The distribution coefficient of the neodymium ion at the structural sites of gadolinium ion is defined as $K_{Nd} = ([Nd]/([Nd]+[Gd]))_{crystal}/([Nd]/([Nd]+[Gd]))_{solution}$. This can be calculated from the data in Table 1 and the stoichiometry of the starting materials. The value (0.984) is very close to 1 because the ionic radius of Nd^{3+} is only slightly bigger than that of Gd^{3+}. This means that the active Nd^{3+} ion can be easily doped in the $KGdP_4O_{12}$ host crystal, and that the composition inside a single crystal would be homogeneous in general.

Table 2. The crystalline forms {hkl} observed in the Nd:$KGdP_4O_{12}$ crystal and the corresponding d_{hkl} arranged by decreasing sense.

{hkl}	d_{hkl} (Å)
{(001) (00$\bar{1}$)}	9.7688
{(110) ($\bar{1}$10) (1$\bar{1}$0) ($\bar{1}\bar{1}$0)}	6.2790
{($\bar{1}$11) (11$\bar{1}$) ($\bar{1}\bar{1}$1) (1$\bar{1}\bar{1}$)}	6.2204
{(010) (0$\bar{1}$0)}	6.1535
{(021) (02$\bar{1}$) (0$\bar{2}$1) (0$\bar{2}\bar{1}$)}	5.2096
{(002) (00$\bar{2}$)}	4.8944

doi:10.1371/journal.pone.0100922.t002

2. Crystal structure

Nd:$KGdP_4O_{12}$ crystallizes in the monoclinic space group $C2/c$ with cell parameters $a = 7.812(2)$ Å, $b = 12.307(3)$ Å, $c = 10.474(2)$ Å, $\beta = 110.84(3)^\circ$ and $Z = 4$. Information regarding crystal data, data collection and refinement is given in Table S1. The atomic coordinate information is given in Table S2, and the anisotropic displacement parameter is given in Table S3. The lengths of P−O, Gd(Nd)−O and K−O bonds are listed in Table S4, and the bond valences have been calculated according to the Brown and Altermatt parameters [30] for the structure of Nd:$KGdP_4O_{12}$. The bond valence sums are reasonable for both cations and anions. The crystal structure of Nd:$KGdP_4O_{12}$ we show here is consistent with that of undoped $KGdP_4O_{12}$ reported by Ettis et al [27]. The Nd^{3+}-active ion occupies the lattice site of Gd^{3+}. The density of a single crystal of Nd:$KGdP_4O_{12}$ at 23°C is 3.54 g·cm^{-3}. This agrees well with the calculated value from the crystallographic data.

The basic structural unit of Nd:$KGdP_4O_{12}$ is a centrosymmetric cyclotetraphosphate ring anion of $[P_4O_{12}]^{4-}$ that is composed of four PO_4 tetrahedra. Each PO_4 tetrahedron shares its two corners (i.e. bridging oxygen) with the others. The four phosphorus atoms of each $[P_4O_{12}]^{4-}$ ring lie in the same plane due to symmetry, and all the oxygen atoms are either above or below the P_4 plane. As shown in projection into the *ac* plane (Figure 2), the $[P_4O_{12}]^{4-}$ rings form layers parallel to (001) at $z = 0$ and 1/2. A previous description [27] suggesting that these layers were perpendicular to the [001] direction is erroneous because the normal of the (001) faces is different from the [001] direction. We note that the $[P_4O_{12}]^{4-}$ rings stack in the structure similar to fish scales. The P_4 plane, i.e. (0.2908, −0.0415, 0.9559), is not parallel to (001), and the interfacial angle between them is 17.08(2)°.

The $Gd(Nd)O_8$ polyhedra and KO_{10} polyhedra link the $[P_4O_{12}]^{4-}$ rings to form a three-dimensional framework. The eight vertexes of the $Gd(Nd)O_8$ polyhedra come from terminal oxygens of the PO_4 polyhedra, and they belong to six $[P_4O_{12}]^{4-}$ rings that are equal in the two adjacent layers. The $Gd(Nd)O_8$ polyhedra do not share any oxygen atoms and are isolated by the PO_4 and KO_{10} polyhedra. Ettis et al [27] erroneously reported the shortest distance between the two rare earth ions to be 5.269 Å. Thus, they thought that it was small compared to the other alkali metal and rare earth tetraphosphates. Actually, the shortest Gd(Nd)−Gd(Nd) distance in the Nd:$KGdP_4O_{12}$ crystal is 6.0059 Å, which is actually relatively long for tetraphosphates.

Figure S1 shows the experimental XRD pattern of the pulverized Nd:$KGdP_4O_{12}$ crystal as well as our simulated pattern. The peak positions and diffraction intensities are consistent between the experimental and simulated XRD patterns. This confirms that our proposed structure is accurate.

For a laser crystal, the mechanical strength is due to the host material. Cleavage behaviour of the host crystal is related not only to the bond strength but also the geometry. There are three kinds of chemical bonds in potassium gadolinium phosphates: P−O, Gd−O and K−O. According to their covalent character, P−O bonds are much stronger than Gd−O and K−O bonds. The K−O bonds are the weakest of all. This is confirmed by the calculated results of bond valences shown in Table S5. The $KGd(PO_3)_4$ structures (both $P2_1$ and $P2_1/n$) are formed by intrachain P−O bonds and interchain Gd−O and K−O bonds. The P−O bonds run along the [100] direction for $KGd(PO_3)_4$ in $P2_1$ and [101] for $KGd(PO_3)_4$ in $P2_1/n$ to generate long chains, respectively. Therefore, the $KGd(PO_3)_4$ crystals have the strongest strength along the above [100] or [101] directions and cleavage very easily occurs between the chains. In $KGdP_4O_{12}$ however, the GdO_8 polyhedra and KO_{10} polyhedra link $[P_4O_{12}]^{4-}$ rings to form a three-dimensional framework, and the strengths along the different directions are quite similar. Therefore, the Nd:$KGdP_4O_{12}$ crystal does not have a prominent cleavage

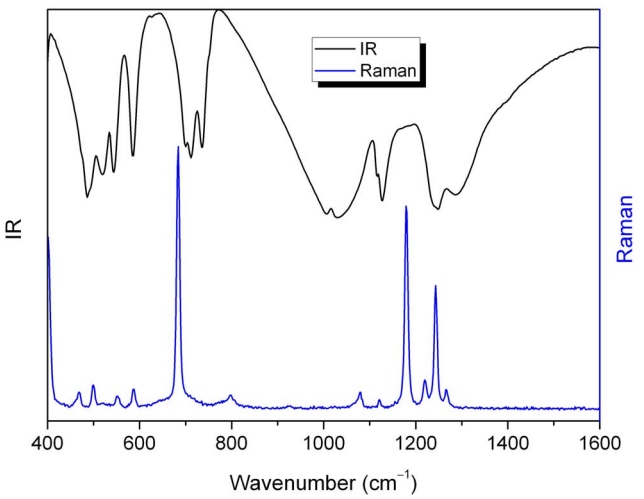

Figure 3. The IR and Raman spectra of Nd:$KGdP_4O_{12}$ at room temperature.
doi:10.1371/journal.pone.0100922.g003

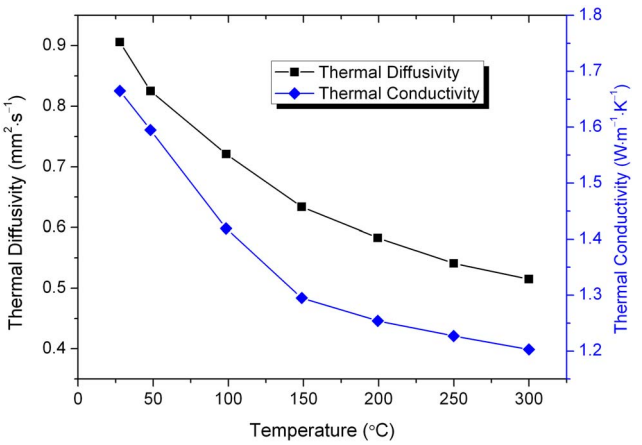

Figure 4. Thermal diffusivities and thermal conductivities of the Nd:$KGdP_4O_{12}$ crystal along the *c direction.**
doi:10.1371/journal.pone.0100922.g004

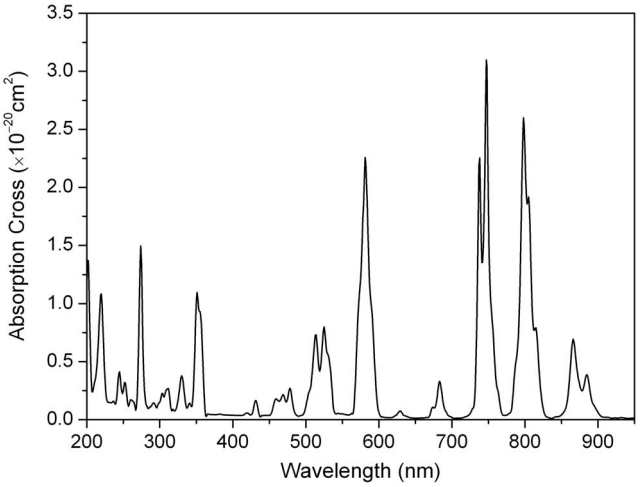

Figure 5. Absorption spectrum of the Nd:$KGdP_4O_{12}$ crystal at room temperature.
doi:10.1371/journal.pone.0100922.g005

behaviour. During the processing of Nd:$KGdP_4O_{12}$ crystals, no crack and cleavage as seen in $KGd(PO_3)_4$ crystals was found.

3. Crystal morphology and rocking curve

The as-grown crystal has some well-developed facets (Figure 1(a)) oriented using an XRD goniometer. The habit contains crystalline forms {001}, {010}, {110} and {021}. The measured interfacial angles among the facets were in good agreement with the calculated angles.

The morphology of a crystal reflects its structure. Taking into account only the point group and the crystal cell parameters, we established the theoretical morphological scheme of the Nd:$KGdP_4O_{12}$ crystal via the WinXMorph software [31] using the Bravais-Friedel and Donnay-Harker (BFDH) law. This morphological scheme is shown in Figure 1(b). Table 2 lists the crystalline forms {hkl}, equivalent faces and corresponding d_{hkl} for Nd:$KGdP_4O_{12}$.

While the as-grown crystal did not show a completely ideal morphology due to the restriction of the crystal growth method, all the predicted crystalline forms can be found on the as-grown single crystal. It should be noted that the $\{\bar{1}11\}$ facet was smaller and limited by the growth conditions. Thus, it was quite pristine and we did not identify $\{\bar{1}11\}$ for the as-grown crystal. The narrow tetragonal facet (021) on the as-grown crystal shows that {021} has a faster growth rate, which is consistent with the predicted scheme. The ideal morphology of $KGdP_4O_{12}$ is like a drum and hexagonal {001} facets reveal much more than other facets similar to drumheads. This relates to the structural feature of $KGdP_4O_{12}$ in which $[P_4O_{12}]^{4-}$ rings regularly array to form layers parallel to (001). The distance between the two $[P_4O_{12}]^{4-}$ rings adjacent to the two layers is larger than that from the same layer.

The rocking curve of the (004) diffraction plane of the as-grown Nd:$KGdP_4O_{12}$ crystal is presented in Figure S2. The diffraction peak is intense and with good symmetry without splitting, and its FWHM value is 0.006°. These results demonstrate that the as-grown Nd:$KGdP_4O_{12}$ crystal has a nearly perfect lattice structure.

4. IR and Raman spectra

The IR and Raman spectra of Nd:$KGdP_4O_{12}$ at room temperature are shown in Figure 3. The vibration frequencies above 600 cm^{-1} and their corresponding assignment are listed in Table S5 and are based on published findings [27,32]. In the low-frequency region below 600 cm^{-1}, it is very difficult to distinguish the symmetric and antisymmetric bending modes of the O−P−O and P−O−P groups.

Compared to other cyclotetraphosphate compounds, we notice an absence of bands in the 750−1000 cm^{-1} region of the IR spectrum. This result is in agreement with the cyclic structure of Nd:$KGdP_4O_{12}$. The non-coincidence of the observed bands in the IR and Raman spectra indicates that the $[P_4O_{12}]^{4-}$ anion is centrosymmetric, which is in agreement with the above structural results.

A distinguishing characteristic also exits in the Raman spectrum. The symmetric stretching vibration of the P−O−P linkage–ν_s(P−O−P)–has a single peak at 684 cm^{-1}. This is the strongest of all the Raman vibration peaks. However, for ν_s(P−O−P) of $KGd(PO_3)_4$ ($P2_1$), two peaks are observed in the range of 660–730 cm^{-1} and have the same intensity [24]. These are less than one half of the intensity of the ν_s(O−P−O). That is because of the symmetrical difference in the crystal structures and the different positions of the lanthanide and alkali ions. The obvious differences between the IR and Raman spectra of $KGdP_4O_{12}$ and $KGd(PO_3)_4$ highlight how IR and Raman spectroscopy can identify the structure of alkali-metal lanthanide metaphosphates.

Table 3. The barycenter wavelength, experimental and calculated oscillator strengths, and absorption cross section of the Nd:$KGdP_4O_{12}$ crystal at room temperature.

$\bar{\lambda}$ (nm)	$^4I_{9/2}\rightarrow J$ manifold	f_{exp} ($\times 10^{-6}$)	f_{cal} ($\times 10^{-6}$)	σ ($\times 10^{-20}$ cm^2)
874	$^4F_{3/2}$	2.04	2.04	0.68
802	$^4F_{5/2}+{}^2H_{9/2}$	7.86	7.82	2.59
745	$^4F_{7/2}+{}^4S_{3/2}$	8.75	8.79	3.09
683	$^4F_{9/2}$	0.80	0.66	0.32
581	$^4G_{5/2}+{}^2G_{7/2}$	11.46	11.46	2.25
520	$^2K_{13/2}+{}^4G_{7/2}+{}^4G_{9/2}$	4.98	5.00	0.79
470	$^2K_{15/2}+{}^2G_{9/2}+{}^2D_{3/2}+{}^4G_{11/2}$	1.34	1.26	0.26
431	$^2P_{1/2}$	0.45	0.47	0.15
353	$^4D_{3/2}+{}^4D_{5/2}+{}^2I_{11/2}+{}^4D_{1/2}$	9.49	9.52	1.09

doi:10.1371/journal.pone.0100922.t003

Table 4. The calculated spontaneous emission probability, radiative branching ratios, radiative lifetime and experimental branching ratios of $^4F_{3/2}$ multiplet of Nd^{3+} in the Nd:$KGdP_4O_{12}$ crystal.

Transition	$^4F_{3/2}\rightarrow{}^4I_{9/2}$	$^4F_{3/2}\rightarrow{}^4I_{11/2}$	$^4F_{3/2}\rightarrow{}^4I_{13/2}$	$^4F_{3/2}\rightarrow{}^4I_{15/2}$
A (s^{-1})	1112	1705	366	17
β_{cal} (%)	34.8	53.3	11.4	0.5
β_{exp} (%)	28.6	58.8	12.6	–
τ_r ($\times10^{-6}$ s)	312			

doi:10.1371/journal.pone.0100922.t004

5. Thermal properties

Generally, double phosphate compounds are not stable at high temperatures. To measure the decomposition, a TG−DSC analysis for the Nd:$KGdP_4O_{12}$ crystal was performed. The TG−DSC curves of the Nd:$KGdP_4O_{12}$ crystal are given in Figure S3. A single sharp endothermic peak is observed at 920°C, which exhibits the characteristics of a first-order phase transition. The sample weight of Nd:$KGdP_4O_{12}$ does not show representative variation in the measurement temperature up to 1000°C. Apart from a crystalline phase, an amorphous phase was formed in the sample cell after the DSC measurement. The $M^{I}Ln^{III}P_4O_{12}$ compounds often decompose irreversibly into lanthanide trimetaphosphates and alkali metal metaphosphates [33]. We thus conclude that the exothermic peak at 920°C may be related to a decomposition of Nd:$KGdP_4O_{12}$ in accordance with the reaction:

$$KGdP_4O_{12}(s)\rightarrow GdP_3O_9(s)+KPO_3(l)$$

The decomposition temperature of the Nd:$KGdP_4O_{12}$ crystal is much higher than that of $KGd(PO_3)_4$ ($P2_1$) (878°C) [20]. The difference in stability between these two potassium gadolinium metaphosphates can be explained by comparing their crystal data. The lengths of P−O bonds vary from 1.4752 to 1.6009 Å for $KGdP_4O_{12}$. However, the P−O bond lengths vary from 1.4414 to 1.6886 Å for $KGd(PO_3)_4$. That is, the PO_4 tetrahedra in $KGd(PO_3)_4$ are heavily distorted as are the GdO_8 polyhedra. The Gd(Nd)−O distances in the Nd:$KGdP_4O_{12}$ are from 2.3665 to 2.4189 Å with an average of 2.3933 Å. The Gd−O distances in $KGd(PO_3)_4$ vary widely from 2.2903 to 2.4767 Å with an average of 2.4059 Å. In addition, the volume per formula of $KGdP_4O_{12}$ (235.3 $Å^3$) is smaller than that of $KGd(PO_3)_4$ (240.4 $Å^3$). Thus, the thermal stability of the cyclic $C2/c$ space group should be better than that of the chain structure in the $P2_1$ space group.

For laser crystal materials, the damage threshold and possible laser applications can be greatly influenced by the specific heat. The specific heat is also an important value used to calculate thermal conductivity. Figure S4 shows that the constant pressure specific heat of the Nd:$KGdP_4O_{12}$ crystal varies as a function of the temperature. The specific heat of the Nd:$KGdP_4O_{12}$ crystal at room temperature (25°C) is 0.521 $J\cdot g^{-1}\cdot K^{-1}$. This is comparable to Nd:YAG (0.59 $J\cdot g^{-1}\cdot K^{-1}$) and Nd:$YVO_4$ (0.51 $J\cdot g^{-1}\cdot K^{-1}$) [34]. Because Nd:YAG and Nd:YVO_4 both have a high optical damage threshold, it follows that Nd:$KGdP_4O_{12}$ should also have a high damage threshold [5]. The specific heat increases almost linearly from 0.485 to 0.799 $J\cdot g^{-1}\cdot K^{-1}$ with temperature increases from −10 to 510°C. This suggests that the Nd:$KGdP_4O_{12}$ crystal can tolerate even more thermal energy at a high temperature.

Figure 4 shows the thermal diffusivity and thermal conductivity of the Nd:$KGdP_4O_{12}$ crystal. The thermal conductivity (κ) was calculated using the measured thermal diffusivity and specific heat according to $\kappa=\lambda\rho C_p$, where λ, ρ and C_p denote the thermal diffusivity, density and specific heat of the crystal at the same temperature, respectively. The thermal diffusivity of the crystal is 0.906 $mm^2\cdot s^{-1}$ along the direction perpendicular to (001), i.e. the c^* direction, at 27.8°C. The calculated thermal conductivity of the crystal is 1.66 $W\cdot m^{-1}\cdot K^{-1}$ along the c^* direction correspondingly. This value is similar to that of Nd:$SrLaGa_3O_7$ [4] and larger than those of some laser crystals with broad absorption such as $NaLn(WO_4)_2$ [2,3] and $Ca_3La_2(BO_3)_4$ [5]. In laser designs, the thermal loading causes a temperature gradient in the crystal and leads to thermal expansion that results in thermal lensing and

Table 5. Comparison of spectroscopic properties of the Nd:$KGdP_4O_{12}$ crystal with other Nd^{3+}-doped crystals.

Crystal	Nd:$KGdP_4O_{12}$	Nd:$SrLaGa_3O_7$	Nd:$KBaGd(MoO_4)_3$	Nd:YVO_4	Nd:YAG
Nd^{3+} (at%)	5.0	1.0	0.91	1.0	1.0
Crystal system	Monoclinic	Tetragonal	Monoclinic	Tetragonal	Cubic
Growth method	TSSG	Czochralski	TSSG	Czochralski	Czochralski
Peak absorption wavelength λ_a (nm)	798	808	804	808.7	808
FWHM at λ_a (nm)	14.8	8	9	2	0.7
Peak emission wavelength λ_e (nm)	1057	1061	1069	1064	1064
FWHM at λ_e (nm)	14	14	24	1.1	0.8
Fluorescence lifetime (μs)	300	310	141	84	230
Ref.	This work	[4]	[12]	[41]	[34]

doi:10.1371/journal.pone.0100922.t005

other thermo-optic effects. All these effects would cause a decline in the quality of the laser beams and even crack the active crystal. The deposited heat would be easily transferred to the environment if the laser crystal possesses high thermal conductivity–this would minimize the thermal loading effects.

It is clearly shown in Figure 4 that the thermal diffusivity and thermal conductivity component of the Nd:$KGdP_4O_{12}$ crystal decreases with increasing temperature. Thermal conductivity is dominated primarily by its phonon thermal conductivity for the dielectric. This has two important determinants: the heat capacity and the phonon mean free path. Though the heat capacity of the Nd:$KGdP_4O_{12}$ crystal increases with temperature, the phonon-phonon scattering becomes much stronger and the phonon mean free path markedly decreases. Therefore, the final result is that the thermal conductivity decreases with temperature increases.

6. Absorption spectrum

Figure 5 shows the unpolarized absorption spectrum of the Nd:$KGdP_4O_{12}$ crystal at room temperature. The UV cut off is below 200 nm. This means that a large band gap would increase the damage resistivity of the crystal. All absorption lines are due to the $4f^3$–$4f^3$ transition of the Nd^{3+} ions. Very strong absorption lines occur near 581, 747 and 798 nm, corresponding to the transitions of $^4I_{9/2}\rightarrow{}^2G_{7/2}+{}^4G_{5/2}$, $^4I_{9/2}\rightarrow{}^4S_{3/2}+{}^4F_{7/2}$ and $^4I_{9/2}\rightarrow{}^2H_{9/2}+{}^4F_{5/2}$, respectively. The interesting feature of this spectrum relative to the potential application in the diode-pumped laser, is the strong absorption band with a FWHM of 14.8 nm near 798 nm. This is close to the laser output of the AlGaAs laser diode. It is well known that temperature control of the laser diode is crucial, because the emission wavelength increases with temperature. Large line-width in the Nd:$KGdP_4O_{12}$ crystal is very suitable for laser diode pumping because it is not temperature dependent.

The Judd-Ofelt theory was used to calculate the optical parameters of the electric dipole transition within the $4f$ electronic configuration of the Nd^{3+} ion. Important parameters included the oscillator intensity parameters (Ω_λ), spontaneous emission probability (A), fluorescence branching ratio (β) and radiative lifetime (τ_r) [35,36]. A detailed calculation procedure was used similar to literature [37]. Nine absorption bands were used to obtain the intensity parameters ($\Omega_{2,4,6}$), which are $\Omega_2 = 1.79\times10^{-20}\,cm^2$, $\Omega_4 = 3.48\times10^{-20}\,cm^2$ and $\Omega_6 = 6.05\times10^{-20}\,cm^2$, respectively. The values of the experimental (f_{exp}) and calculated (f_{cal}) oscillator strengths are listed with the absorption cross sections (σ) in Table 3. The root mean square error (δ) between f_{exp} and f_{cal} is 6.97×10^{-8}. The properties of $^4F_{3/2}\rightarrow{}^4I_J$ ($J = 9/2,\ 11/2,\ 13/2,\ 15/2$) transitions are well known. These are the main channels of a Nd^{3+} laser and depend only on the values of Ω_4 and Ω_6 because the reduced matrix elements $|<||U^{(2)}||>|$ for these transitions are zero. The spectroscopic quality parameter ($X = \Omega_4/\Omega_6$) is 0.57, which is less than 1 and indicates that the emission to the $^4I_{11/2}$ manifold is more feasible than that to $^4I_{9/2}$ manifold. This result can be confirmed by the fluorescence emission spectrum (see below). In this regard, it is similar to the most common laser materials based on the Nd^{3+} ion including Nd:YVO_4 and Nd:YAG. Table 4 presents the spontaneous emission probability (A), radiative branching ratio (β) and radiative lifetime (τ_r) of the multiplet $^4F_{3/2}$. It can be seen that the calculated branching ratios are in good agreement with the experimental ones obtained from the measured fluorescence spectrum later.

7. Fluorescence spectra analysis

The room temperature fluorescence spectrum of the Nd:$KGdP_4O_{12}$ crystal at 808 nm excitation was recorded from 830 to 1600 nm (Figure 6). Three emission bands corresponding to the $^4F_{3/2}\rightarrow{}^4I_{9/2}$, $^4I_{11/2}$ and $^4I_{13/2}$ transitions are observed at 860–920 nm, 1040–1080 nm and 1300–1380 nm, respectively. The room temperature emission FWHM of the transition $^4F_{3/2}\rightarrow{}^4I_{11/2}$ is 14 nm. This is evidence of the dominant contribution of inhomogeneous broadening to the spectra line-width in the low symmetry structure. The emission cross sections for the laser channel from $^4F_{3/2}$ to $^4I_{9/2}$, $^4I_{11/2}$ and $^4I_{13/2}$ were calculated through the Füchtbauer-Ladenburg (FL) formula [12,18]. These values are 1.11×10^{-20}, 6.25×10^{-20} and $2.13\times10^{-20}\,cm^2$, respectively.

The emission spectra of the Nd:$KGdP_4O_{12}$ at low temperature were studied to determine the Stark sublevels of the $^4I_{13/2}$ and $^4I_{11/2}$ excited multiplets and the ground state multiplet $^4I_{9/2}$. Figure S5 shows the emission spectra of Nd:$KGdP_4O_{12}$ at 10K and 300K. These correspond to the transitions from $^4F_{3/2}$ to $^4I_{9/2}$, $^4I_{11/2}$ and $^4I_{13/2}$ levels, respectively. Figure 7 shows a schematic diagram of the Stark sublevels of Nd^{3+} in $KGdP_4O_{12}$ crystals obtained from the low temperature emission spectra. The $^4F_{3/2}$ term is split into two components with $\Delta = 70\ cm^{-1}$. The low value of the crystal field splitting indicates that the crystal field of the $KGdP_4O_{12}$ host is weak. This is due to weak interactions between rare earth ions and oxygen atoms in contrast with the strong covalent bonds between P and O. In this regard, the Nd:$KGdP_4O_{12}$ crystal is similar to other double phosphates of alkali and lanthanide ions [38,39].

The fluorescence lifetime (τ_f) of the $^4F_{3/2}$ energy level of Nd^{3+} in the Nd:$KGdP_4O_{12}$ crystal was determined to be 300 μs by fitting the decay curve exponentially (Figure S6). The long fluorescence lifetime would be beneficial to high energy storage during laser operation. Though the interatomic distance (6.0059 Å) between the nearest rare earth ions for $KGdP_4O_{12}$ is smaller than that for $KGd(PO_3)_4$ ($P2_1$) (6.5865 Å), it does not obviously affect the fluorescence lifetime. This is a function of the isolated GdO_8 polyhedra in $KGdP_4O_{12}$. The τ_f of the Nd:$KGd(PO_3)_4$ crystal ($P2_1$) is 246 μs with a very low doping concentration (0.6 at%) [38]. The values of Nd:LaP_5O_{14} and Nd:GdP_5O_{14} crystals are around 310 μs when doped with ~1 at% Nd^{3+} [40].

It is well known that the τ_f of Nd^{3+} ions generally decreases with increasing Nd^{3+} concentrations due to the interactions between the Nd^{3+} ions, i.e. the concentration quenching effect. However,

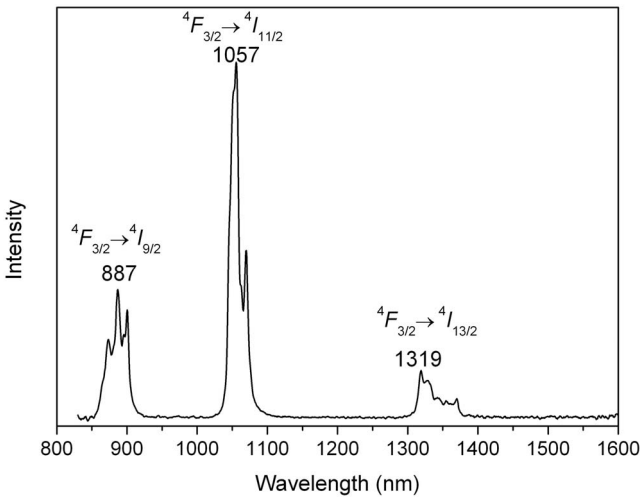

Figure 6. Emission fluorescence spectrum of the Nd:$KGdP_4O_{12}$ crystal at room temperature.
doi:10.1371/journal.pone.0100922.g006

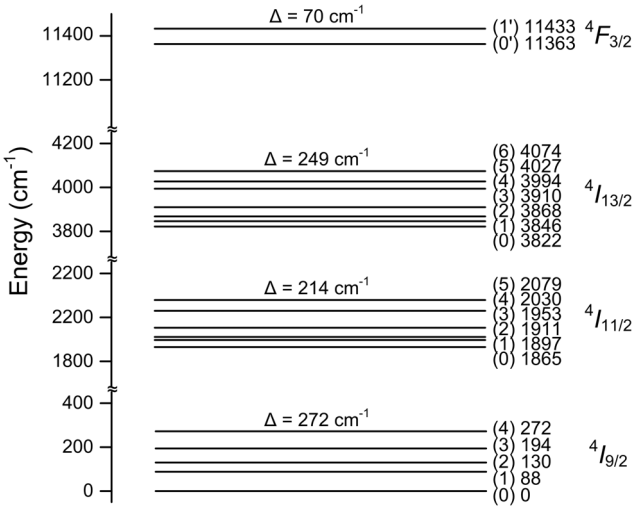

Figure 7. Stark structure of the energy levels of the Nd^{3+} ion in the $KGdP_4O_{12}$ crystal.
doi:10.1371/journal.pone.0100922.g007

the Nd:$KGdP_4O_{12}$ crystal still has a long fluorescence lifetime of 300 μs under a higher doping concentration of 5 at%. Versus the above phosphates, the $KGdP_4O_{12}$ crystal is a distinct laser host material with a very low concentration quenching for Nd^{3+} because the Nd:$KGdP_4O_{12}$ crystal ensures a long fluorescence lifetime even under a high active ion concentration.

The calculated τ_r of the $^4F_{3/2}$ energy level is 312 μs (Table 4). Thus, the fluorescent quantum efficiency ($\eta = \tau_f/\tau_r$) of the $^4F_{3/2}$ level is 96%. For solid-state laser materials, low crystal field strength leads to weak electron-phonon interactions and further leads to high quantum efficiency. The previous data describing weak Stark splitting of the Nd^{3+} energy levels further supports the calculated result showing that Nd:$KGdP_4O_{12}$ has a high quantum efficiency.

Some spectroscopic properties of the Nd:$KGdP_4O_{12}$ crystal are listed in Table 5 as well as those of other Nd^{3+}-doped crystals including YAG and YVO_4 crystals with ordered structures and $SrLaGa_3O_7$ and $KBaGd(MoO_4)_3$ crystals with disordered structures. The FWHM value of Nd:$KGdP_4O_{12}$ at λ_a is not only much larger than those of Nd:YAG and Nd:YVO_4 crystals, but also larger than those of Nd:$SrLaGa_3O_7$ and Nd:$KBaGd(MoO_4)_3$ crystals. This suggests that the Nd:$KGdP_4O_{12}$ crystal can be pumped more effectively by AlGaAs laser diode, but not be restricted to the temperature stability of the output wavelength in the laser diode. The quality factor (M) of a laser material is proportional to its doping concentration (N) and fluorescence lifetime (τ_f). A high value of M generally means a low oscillation threshold in subsequent laser operations. Therefore, the high doping concentration and long fluorescence lifetime of Nd:$KGdP_4O_{12}$ makes it possible to achieve a continuous wave laser action. In addition, Nd:$KGdP_4O_{12}$ can be used as a tunable laser material with a very broad emission band near 1060 nm.

Conclusions

We successfully grew a macro-defect-free single crystal of 5 at% Nd^{3+}-doped $KGdP_4O_{12}$ with very good crystallinity using TSSG−SC from self-flux. To the best of our knowledge, both the growth of the bulk crystals and doping with neodymium are shown here for the first time in $KGdP_4O_{12}$. The Nd:$KGdP_4O_{12}$ crystallizes in space group $C2/c$, and the phosphoric anions have a cyclic geometry of $[P_4O_{12}]^{4-}$. The crystal has good chemical stability and does not show cleavage like its isomer $KGd(PO_3)_4$. The distribution coefficient of neodymium ion is very close to 1, so gadolinium ion can be evenly substituted. The absorption and fluorescence spectra of the Nd:$KGdP_4O_{12}$ crystal were investigated at room temperature. The peak absorption cross section at 798 nm is 2.59×10^{-20} cm^2 with a FWHM of 14.8 nm. Such a broad FWHM in the absorption band is suitable for InGaAs laser diode pumping. The radiation and fluorescence lifetimes of the excited state $^4F_{3/2}$ are 312 and 300 μs, respectively. These result in a high luminescent quantum efficiency of 96%. The emission from the $^4F_{3/2}$ energy level to the $^4I_{11/2}$ manifold is more feasible than that of the $^4I_{9/2}$ manifold. The peak emission cross section at 1057 nm (corresponding to $^4F_{3/2}\rightarrow{}^4I_{11/2}$) is 6.25×10^{-20} cm^2. In addition, the $KGdP_4O_{12}$ crystal presents positive thermal characteristics. It has a good thermal stability with decomposition at 920°C. At room temperature, the specific heat and the thermal conductivity along the c^* direction are 0.521 $J\cdot g^{-1}\cdot K^{-1}$ and 1.66 $W\cdot m^{-1}\cdot K^{-1}$, respectively. In summary, the Nd:$KGdP_4O_{12}$ crystal may be regarded as a potential solid-state laser material for laser diode pumping.

Supporting Information

Figure S1 The experimental XRD pattern of Nd:$KGdP_4O_{12}$ from polycrystalline powder and the simulated pattern from single crystal data.
(DOCX)

Figure S2 XRD rocking curve of the (004) diffraction plane of the as-grown Nd:$KGdP_4O_{12}$ single crystal.
(DOCX)

Figure S3 TG and DSC curves of the Nd:$KGdP_4O_{12}$ crystal.
(DOCX)

Figure S4 Specific heat versus temperature curve of the Nd:$KGdP_4O_{12}$ crystal.
(DOCX)

Figure S5 Emission fluorescence spectra of the Nd:$KGdP_4O_{12}$ crystal at 10K and 300K.
(DOCX)

Figure S6 Fluorescence decay curve of the $^4F_{3/2}$ manifold of the Nd:$KGdP_4O_{12}$ crystal at room temperature.
(DOCX)

Table S1 Crystal data, data collection and refinement of Nd:$KGdP_4O_{12}$.
(DOCX)

Table S2 Atomic coordinates and equivalent isotropic displacement parameters of Nd:$KGdP_4O_{12}$.
(DOCX)

Table S3 Anisotropic displacement parameters ($Å^2$) of Nd:$KGdP_4O_{12}$.
(DOCX)

Table S4 Bond lengths and bond valences in the Nd:$KGdP_4O_{12}$ crystal.
(DOCX)

Table S5 Frequencies (cm^{-1}) and assignments of IR absorption and Raman scattering for Nd:$KGdP_4O_{12}$.
(DOCX)

Acknowledgments

The authors thank Dr. Shifeng Jin (Institute of Physics, Chinese Academy of Science) for his help in the rocking curve measurements.

Author Contributions

Conceived and designed the experiments: TS YK JX. Performed the experiments: TS YZ. Analyzed the data: TS YZ PS ZZ. Contributed reagents/materials/analysis tools: TS SC. Wrote the paper: TS.

References

1. Kaminskii AA (2007) Laser crystals and ceramics: recent advances. Laser & Photon Rev 1: 93–177.
2. Faure N, Borel C, Couchaud M, Basset G, Templier R, et al. (1996) Optical properties and laser performance of neodymium doped scheelites $CaWO_4$ and $NaGd(WO_4)_2$. Appl Phys B 63: 593–598.
3. Cheng Z, Zhang S, Fu K, Cheng H (2001) Growth, thermal and laser properties of neodymium doped sodium yttrium double tungstate crystal. Jpn J Appl Phys 40: 4038–4040.
4. Zhang YY, Zhang HJ, Yu HH, Sun SQ, Wang JY, et al. (2011) Characterization of disordered melilite Nd:$SrLaGa_3O_7$ crystal. IEEE J Quantum Elect 47: 1506–1513.
5. Pan ZB, Cong HJ, Yu HH, Tian L, Yuan H, et al. (2013) Growth, thermal properties and laser operation of Nd:$Ca_3La_2(BO_3)_4$: a new disordered laser crystal. Opt Express 21: 6091–6100.
6. Li H, Zhang LZ, Wang GF (2009) Growth, structure and spectroscopic characterization of a new laser crystals Nd^{3+}:$Li_3Ba_2Gd_3(WO_4)_8$. J Alloy Compd 478: 484–488.
7. Li H, Wang GJ, Zhang LZ, Huang YS, Wang GF (2010) Growth and structure of Nd^{3+}-doped $Li_3Ba_2Y_3(WO_4)_8$ crystal with a disorder structure. CrystEngComm 12: 1307–1310.
8. Xiao B, Zhang LZ, Lin ZB, Huang YS, Wang GF (2012) Growth and spectral properties of Nd^{3+}:$Li_3Ba_2La_3(WO_4)_8$ crystal. Optoelectron Adv Mat 6: 404–410.
9. Song MJ, Wang GJ, Lin ZB, Zhang LZ, Wang GF (2007) Growth and spectral properties of Nd^{3+}-doped $Li_3Ba_2Y_3(MoO_4)_8$ crystal. J Cryst Growth 308: 208–212.
10. Song MJ, Zhang LZ, Wang GF (2009) Growth and spectral properties of Nd^{3+}-doped $Li_3Ba_2Ln_3(MoO_4)_8$ (Ln = La, Gd) crystals. J Alloy Compd 480: 839–842.
11. Song MJ, Zhao W, Wang GF, Zhao ML, Wang LT (2011) Growth, thermal and polarized spectral properties of Nd^{3+}-doped $Li_3Ba_2Gd_3(MoO_4)_8$ crystal. J Alloy Compd 509: 2164–2169.
12. Meng XM, Lin ZB, Zhang LZ, Huang YS, Wang GF (2011) Structure and spectral properties of Nd^{3+}-doped $KBaGd(MoO_4)_3$ crystal with a disorder structure. CrystEngComm 13: 4069–4073.
13. Xiao B, Huang YS, Zhang LZ, Lin ZB, Wang GF (2012) Growth, structure and spectroscopic characterization Nd^{3+}-doped $KBaGd(WO_4)_3$ crystal with a disordered structure. PLoS ONE 7: e40229.
14. Cheng Y, Xu XD, Xin Z, Yang XB, Xiao XD, et al. (2009) Crystal growth, optical properties, and continuous-wave laser operation of Nd^{3+}-doped $CaNb_2O_6$ crystal. Laser Phys Lett 6: 740–745.
15. Xu XD, Cheng SS, Meng JQ, Li DZ, Zhou DH, et al. (2010) Spectral characterization and laser performance of a mixed crystal Nd:$(Lu_xY_{1-x})_3Al_5O_{12}$. Opt Express 18: 21370–21375.
16. Li DZ, Xu XD, Zhou DH, Zhuang SD, Wang ZP, et al. (2010) Crystal growth, spectral properties, and laser demonstration of laser crystal Nd:LYSO. Laser Phys Lett 7: 798–804.
17. Li DZ, Xu XD, Cong ZH, Zhang J, Tang DY, et al.(2011) Growth, spectral properties, and laser demonstration of Nd:GYSO crystal. Appl Phys B 104: 53–58.
18. Li DZ, Xu XD, Zhang J, Cong ZH, Tang DY, et al. (2011) Growth, spectral properties, and laser demonstration of Nd:$(Lu_{0.5}Gd_{0.5})_2SiO_5$ crystal. Laser Phys Lett 8: 647–652.
19. Boulon G (2003) Yb^{3+}-doped oxide crystals for diode-pumped solid state lasers: crystal growth, optical spectroscopy, new criteria of evaluation and combinatorial approach. Opt Mat 22: 85–87.
20. Parreu I, Solé R, Gavaldà J, Massons J, Díaz F, et al. (2005) Crystal growth, structural characterization, and linear thermal evolution of $KGd(PO_3)_4$. Chem Mater 17: 822–828.
21. Parreu I, Carvajal JJ, Solans X, Díaz F, Aguiló M (2006) Crystal structure and optical characterization of pure and Nd-substituted type III $KGd(PO_3)_4$. Chem Mater 18: 221–228.
22. Parreu I, Solé R, Gavaldà J, Massons J, Díaz F, et al. (2003) Crystallization region, crystal growth, and phase transitions of $KNd(PO_3)_4$. Chem Mater 15: 5059–5064.
23. Parreu I, Solé R, Massons J, Díaz F, Aguiló M (2007) Crystal growth, crystal morphology and surface micromorphology of type III $KGd(PO_3)_4$ and $KNd(PO_3)_4$. Cryst Growth Des 7: 557–563.
24. Parreu I, Solé R, Massons J, Díaz F, Aguiló M (2007) Crystal growth and characterization of type III ytterbium-doped $KGd(PO_3)_4$: a new nonlinear laser host. Chem Mater 19: 2868–2876.
25. Parreu I, Pujol MC, Aguiló M, Díaz F, Mateos X, et al. (2007) Growth, spectroscopy and laser operation of Yb:$KGd(PO_3)_4$ single crystals. Opt Express 15: 2360–2368.
26. Solé R, Ruiz X, Pujol MC, Mateos X, Carvajal JJ, et al. (2009) Physical properties of self-flux and WO_3-containing solutions useful for growing type III $KGd(PO_3)_4$ single crystals. J Cryst Growth 311: 3656–3660.
27. Ettis H, Naïli H, Mhiri T (2003) Synthesis and crystal structure of a new potassium-gadolinium cyclotetraphosphate, $KGdP_4O_{12}$. Cryst Growth Des 3: 599–602.
28. Rekik W, Naïli H, Mhiri T (2004) Potassium gadolinium polyphosphate, $KGd(PO_3)_4$. Acta Cryst C60: i50–i52.
29. Zhang JJ, Zhang ZH, Zhang WG, Zheng QX, Sun YX, et al. (2011) Polymorphism of $BaTeMo_2O_9$: a new polar polymorph and the phase transformation. Chem Mater 23: 3752–3761.
30. Brown ID, Altermatt D (1985) Bond-valence parameters obtained from a systematic analysis of the Inorganic Crystal Structure Database. Acta Cryst B41: 244–247.
31. Kaminsky W (2007) From CIF to virtual morphology using the WinXMorph program. J Appl Crystallogr 40: 382–385.
32. Horchani K, Ferid M, Gacon JC, Lecocq S, Trabelsi-Ayedi M, et al. (2002) Structure refinement, infrared and Raman spectra of $KDyP_4O_{12}$. Mater Res Bull 37: 1259–1267.
33. Jungowska W, Znamierowska T (1990) Studies on thermal stability of mixed metaphosphates $KLa(PO_3)_4$ and $K_2La(PO_3)_5$. J Therm Anal Calorim 36: 2095–2098.
34. Koechner W (2006) Solid-State Laser Engineering (6th). New York: Springer Press. 54–73.
35. Judd BR (1962) Optical absorption intensities of rare-earth ions. Phys Rev 127: 750–761.
36. Ofelt GS (1962) Intensities of crystal spectra of rare-earth ions. J Chem Phys 37: 511–520.
37. Wang GF, Chen WZ, Lin ZB, Hu ZS (1999) Optical transition probability of Nd^{3+} ions in a alpha-Nd^{3+}:$LaSc_3(BO_3)_4$ crystal. Phys Rev B 60: 15469–15471.
38. Parreu I (2006) Crystal growth and characterization of ytterbium or neodymium doped type III-KGd(PO3)4-a new bifunctional nonlinear and laser crystal. Tarragona: Rovira i Virgili University. 114.
39. Maksimova SI, Palkina KK, Loshchenov VB (1981) Structure and luminescence properties of α'-$CsNd(PO_3)_4$. Izv Akad Nauk SSSR Nerog Mater 17: 116–120.
40. Weber HP (1975) Nd pentaphosphate lasers. Opt Quant Electron 7: 431–442.
41. Sato Y, Taira T (2005) Comparative study on the spectroscopic properties of Nd:$GdVO_4$ and Nd:YVO_4 with hybrid process. IEEE J Sel Top Quantum Electron 11: 613–620.